Comparison of 14C and 210Pb - 137Cs - 241Am dating methods of a recent bat guano deposit (Lot, SW France)

Michel Condomines, Ilham Bentaleb, Eleni Filaiti, Aloïs Robert, Claude Milhas

Version of Record: https://www.sciencedirect.com/science/article/pii/S1871101422001480
Manuscript_f2d46ef09638dd0566bd1a753df20c47

Comparison of ^{14}C and ^{210}Pb - ^{137}Cs - ^{241}Am dating methods of a recent bat guano deposit (Lot, SW France).

Michel Condomines[1*], Ilham Bentaleb[2], Eleni Filaiti[2], Aloïs Robert[3], Claude Milhas[4]

1 Univ Montpellier, Univ Antilles, CNRS. Géosciences. Montpellier, France

2 Univ Montpellier, CNRS, IRD, EPHE, CIRAD, INRAP. Montpellier, France

3 Yale University - Department of Ecology and Evolutionary Biology Environmental , New Haven, CT 06511, USA

4 Comité Départemental de Spéléologie du Lot, Montfaucon, France

Abstract:

Bat guano deposits are increasingly used as records of past environmental changes, an approach that requires a precise chronology of the guano layers. This paper presents a comparison between the well-established ^{14}C dating method and methods based on natural ^{210}Pb excesses, $(^{210}Pb)_{ex}$, and artificial radionuclides ^{137}Cs and ^{241}Am. The studied example is a bat guano deposit from a cave in SW France (the Brantites III cave), which is currently investigated for paleo-environmental reconstructions using stable isotopes. ^{14}C data show that the upper part of the guano deposit accumulated during the last 150 years with a marked increase in accumulation rates after around 1960 AD. While the incorporation of atmospheric ^{14}C in guano is a well-understood process, the origin of ^{210}Pb excesses is more complex. Based on consideration of ^{137}Cs and $(^{210}Pb)_{ex}$ inventories recorded in undisturbed soils in France, and the measured inventories in the guano deposit, we suggest that most of the ^{210}Pb excess is produced by ^{222}Rn decay in the cave air and then adsorbed onto the guano. As Radon concentrations in caves can vary significantly on both short and long-term timescales, one needs to be cautious before applying the often-used CRS (constant rate of supply of ^{210}Pb excess) model to guano dating. Our $(^{210}Pb)_{ex}$ data are best interpreted by two successive periods of roughly constant, but widely different accumulation rates (0.3 m/y and 2.6 cm/y before and after 1960, respectively) and $(^{210}Pb)_{ex}$ fluxes. We suggest that these relatively abrupt variations result from a change in cave ventilation leading to a more favourable shelter for bats after 1960. The upper 40 cm of the deposit shows evidence of ^{210}Pb mobility, adding a further complexity to the interpretation of $(^{210}Pb)_{ex}$ profiles in guano deposits. However, the existence of well-defined ^{137}Cs and ^{241}Am peaks allows a precise identification of the year of

maximum atmospheric fallouts (~ 1963-1964). When the ages provided by artificial radionuclides are combined with the ^{210}Pb-derived accumulation rates, an age model can be built, which is in good agreement with the ^{14}C age model. This example shows that the (^{210}Pb)$_{ex}$ method, when associated with ^{137}Cs (^{241}Am) data, can be used to date recent guano deposit, although its application is not as straightforward as the ^{14}C method.

* Corresponding author: michel.condomines@umontpellier.fr

Université de Montpellier, place Eugène Bataillon, 34095 Montpellier cedex 05, France

Keywords: cave guano deposits; ^{14}C ages; ^{210}Pb, ^{137}Cs, ^{241}Am dating; age models; ^{210}Pb flux and cave ventilation.

1 Introduction

Reconstruction of paleoenvironments and paleoclimates are based on many types of natural archives, such as, for example, lacustrine or marine sediments, loess deposits, ice cores, or speleothems. After the pioneering work of DesMarais et al. (1980), several studies have emphasized the interest of bat guano deposits found in a number of caves as records of past climatic and environmental changes, (e.g. Wurster et al., 2008; Johnston et al., 2010; Ferenc et al., 2015). In order to date these changes and compare various records, a precise chronology for such deposits is required. Wurster et al. (2009) showed that bat organic rich guano material can be successfully dated through the ^{14}C method. Another possible chronometer for young deposits (less than 150 y old) is ^{210}Pb. While the ^{210}Pb dating method is widely used to infer sedimentation rates and ages of young sediments, few works tried to apply this method to guano deposits. Among them are those of Wirrmann et al. (2014) and Gallant et al. (2020), whose results are further discussed by Bogdanovicz et al. (2020). Wirrmann et al. (2014) analysed bat and salangane guano from New Caledonia and found a simple $(^{210}Pb)_{ex}$ vs depth profile, allowing them to infer an accumulation rate of 3.5 cm/y. In contrast Gallant et al. (2020) obtained a more complex profile in a guano deposit from Jamaica, and the dates derived from ^{210}Pb are sometimes in conflict with those given by the ^{14}C method. In a recent study, McFarlane and Lundberg (2021) showed that ^{210}Pb (and ^{137}Cs) can be mobile in bat guano, a process that can seriously affect the chronology based on these elements.

In this paper, we assess the potential of ^{210}Pb and ^{137}Cs, ^{241}Am as dating tools for recent bat guano deposits and compare the results with those of the well-established ^{14}C method. The studied example is a bat guano deposit found in a cave from SW France (Brantites III cave, Lot), which is currently being investigated for paleo-environmental reconstructions using stable isotopes.

2 Site description and sampling

Numerous caves and vertical pits (avens or “igues”) are found in the Causse du Quercy area, an upper-Jurassic calcareous plateau, west of the French Massif Central, and part of the sedimentary Aquitaine Basin. The Brantites I and II caves are located near the village of Caniac-du-Causse at an altitude of 259 m a.s.l. Meteorological data are available from the Gourdon station, located about 25 km to the NW. The Brantites III cave is connected to the

larger Brantites I cave, with an opening in the vertical Brantites I pit, a small un-explored gallery at the opposite end, and a small aperture at the surface of the Causse (see map of Fig. 1). The Brantites I and II caves were first explored and described by the founder of speleology E.A. Martel (Martel, 1894).

Observations made during the last decades show that the Brantites III cave is home to 1000 to 3000 insectivorous bats (3 rhinoloph species) during the birthing period (mostly from June to September). Over the years a guano heap around 1.75 m high has accumulated (Fig. 2). The guano deposit is located around 7m below the land-surface. The top of the guano heap was probably deposited in 2011 or 2012, since no bats were observed in the cave in 2013 and 2014, although they were back in the cavity in 2015.

A vertical section was cut in the guano deposit with a shovel in March 2014. In the upper part, alternating layers of light and dark brown colours can be easily seen, whereas the layering tends to disappear below 80 cm depth. The lowermost part of the guano heap (below 120 cm) has a dark brown colour and appears more compact (Fig. 2a). Four cores (C1 to C4) were sampled using PVC half-pipes of 9 cm internal diameter. Their staggered arrangement with a 20 cm overlap between each core was intended to avoid gaps in the record. However this choice resulted in some difficulties in assessing the depth of a given layer along the axis of the guano heap, where the layers are roughly horizontal. Thus approximate corrections have been applied to take into account the dip and thickness variations of the guano layers. This recalculated axial depth is reported in the following tables and diagrams.

3 Sample preparation and analytical methods

In the laboratory the guano cores were cut into 1cm-thick slices, put in plastic bags and stored in a freezer. Eight samples of about 1 cm^3 each were subsampled and sent to Poznań Laboratory for Radiocarbon dating (Goslar et al., 2004). The guano is a mixture of digested organic matter, remains of insect parts (essentially made of chitine), and bat's hair. As all complex organic materials, guano samples require a pre-treatment before AMS analyses. The method used is adapted from that described by Brock et al. (2010), and briefly summarised by Johnston et al. (2010). The procedure involves treatments with acid and base solutions, preceded by treatment with DCM/alcohol to get the fraction of SEG (solvent-extracted guano) free of saturated hydrocarbons (Wurster et al. 2009). Guano samples are then combusted to CO_2, and the CO_2 is finally reduced with H_2, using Fe powder as a catalyst, the final product

to be analysed being a mixture of carbon and iron (C/Fe = 1/2) pressed into a 1 mm hole in an aluminium cathode holder. The carbon isotope composition is determined on a "Compact Carbon AMS", manufactured by National Electrostatics Corporation, USA (detailed procedures for AMS analyses are given by Goslar et al. (2004).

For ^{210}Pb and ^{137}Cs, ^{241}Am analyses, the samples were dried in an oven, for about one day at 60°C. The dried samples were then weighted, in order to estimate the "dry bulk density" DBD (i.e. the dry weight divided by the volume of 1 cm-thick layer). The dry weights of the layers were highly variable, from 2.8 to 6.5 g, with an average value of 4.4 g, i.e. an average DBD of 0.138 g/cm^3. Weight variations are partly due to the difficulty of cutting regular slices in this heterogeneous guano material and to variable proportions of its components. However, there is no systematic increase of the DBD with depth, suggesting that compaction does play a minor role in the studied part of the guano deposit.

The samples were then crushed in an agate mortar and homogenized. The powdered samples were put in PE tubes of 14 mm internal diameter filled to a height of 39 mm for their analysis by gamma spectrometry in a low-background Ge-well detector manufactured by CANBERRA^{TM}. An average 2.7 g (from 2.1 to 3.7 g) was analysed in this way. ^{210}Pb activities in guano samples were determined using its 46.5 keV gamma-ray by comparison of their count rates with that of the ^{210}Pb peak of an in-house standard (volcanic rock) in which activities of the U-series nuclides are well known. The efficiency calibration curve (absolute efficiency vs gamma energy) obtained from this rock standard was used to calculate the activities of ^{241}Am (at 59.5 keV) and ^{137}Cs (at 661.7 keV). Auto-absorption corrections can be significant for low energy peaks such as those of ^{210}Pb and ^{241}Am. The low energy gamma rays are much less absorbed in the guano samples, being essentially composed of light elements (C, H, O, N) and having a low density, than in the volcanic rock standard, and thus a correction has to be applied. The absorption coefficients (μ/ρ) were experimentally determined on a few guano samples by measuring the attenuation of the 46.5 keV (^{210}Pb) and 63.2 keV (^{234}Th) gamma-rays emitted by a small pitchblende (U_3O_8) source, and passing through a box containing the guano samples, using a broad-energy Ge detector BEGe 3825 made by CANBERRA^{TM}. The absorption coefficient for the 59.5 keV peak of ^{241}Am is obtained by interpolation from the above measurements. Calculated auto-absorption correction factors (i.e. the factors by which to multiply the activity/g of a guano sample

derived from the ratio of count rates/g of sample and standard) are about 0.70 and 0.80 for ^{210}Pb and ^{241}Am respectively.

In order to calculate the ^{210}Pb excess ("unsupported" ^{210}Pb), $(^{210}Pb)_{ex}$, ^{226}Ra must also be evaluated. Because of the very low ^{226}Ra activity in most samples, ^{226}Ra was measured using the peak at 352 keV of its progeny ^{214}Pb, and, when possible, also the other peaks of ^{214}Pb (295 keV) and ^{214}Bi (609 keV). As discussed later in section 5.1, this calculated $(^{210}Pb)_{ex}$ does not necessarily represent the true ^{210}Pb adsorbed on the surface of guano. Th content was also estimated using the 238.6 keV peak of its progeny ^{212}Pb, assuming radioactive equilibrium in the ^{232}Th-decay series.

All $^{210}Pb_{ex}$ ($T_{1/2}$ = 22.3 y), ^{137}Cs ($T_{1/2}$ = 30 y) and ^{241}Am ($T_{1/2}$ = 432 y) data, obtained in 2020 and 2021, are decay-corrected to the date of sampling (8 March 2014).

4 Results

4.1 ^{14}C data

^{14}C data and ages obtained on the studied part of the guano deposit are reported in Table 1. Data are expressed in conventional ^{14}C ages BP for samples deposited before 1950, and in pMC (percentage of Modern Carbon) for samples deposited later than 1950. The oldest ^{14}C date is 130 ± 30 BP at a depth of 138 cm. A calibrated date around 1871 ± 72 AD is calculated using the OxCal program (Bronk Ramsey, 2009) in its 4.4 version (2021), with the IntCal20 calibration curve (Reimer et al., 2020), as the mean age of the highest probability interval (1799-1942 AD). All the other layers, above 102 cm were deposited during the period affected by atmospheric nuclear tests, with ^{14}C /^{12}C ratios higher than the reference value of modern (1950 AD) carbon. Expressed in pMC, the values range from 105.9 at 7 cm to 166.6 at 102 cm depth. The pMC values regularly decrease from 97 to 7 cm depth, indicating that these guano layers were deposited after 1964, year of the maximum bomb ^{14}C content in the atmosphere. The dates reported in Table 1 are calculated using the OxCal program and the Bomb21 NH1 calibration curve (Reimer et al., 2020; Hua et al., 2021). The ^{14}C date for the layer at 102 cm depth (166.6 pMC) could correspond to 1966-1967 AD, but our ^{137}Cs data below suggest a date of 1963.3, just before the ^{14}C bomb peak (1963.7). Thus, according to ^{14}C data, the upper 1.50 m of guano accumulated for around 140 years,

from 1870 to 2011, although the accumulation rate was much lower in the bottom part of the guano deposit (36 cm between 1870 and 1963, compared to 102 cm between 1963 and 2011, with an average sedimentation rate of 2.4 cm/y). The age range covered by the ^{14}C dates closely corresponds to the dating interval accessible through the ^{210}Pb method.

4.2 ^{210}Pb, ^{137}Cs and ^{241}Am data

These data are reported in Table 2. Note that, throughout the paper, parentheses denote activities/g. $(^{210}Pb)_{ex}$ activities/g of guano sample are reported vs depth in Fig. 3. Obviously the $(^{210}Pb)_{ex}$ profile does not conform to a simple model assuming a constant initial $(^{210}Pb)_{0,ex}$ activity/g and a constant accumulation rate, that should result in a straight line with a negative slope, when $(^{210}Pb)_{ex}$ is plotted on a logarithmic scale. $(^{210}Pb)_{ex}$ first increase over the depth range 0 to 43 cm, from 59 to 114.5 mBq/g, then shows a roughly linear decrease with a ^{210}Pb of 36 mBq/g at 104.5 cm. This general tendency is however rather irregular. Then, over a few cm (104.5 to 108 cm), $(^{210}Pb)_{ex}$ increases from 36 to 56.5 mBq/g. Finally, in the deepest analysed part of the guano deposit (108 to 138 cm), $(^{210}Pb)_{ex}$ displays a linear decrease until it reaches 4.5 mBq/g, a near zero value within 2σ uncertainty.

^{137}Cs activities are hardly detectable in the upper 45 cm of the guano sequence (≤ 1 mBq/g). They then increase from 63.5 cm (1.17 mBq/g) to reach a peak value of 17.2 mBq/g at 100.5 cm, decreasing thereafter to values lower than 1 mBq/g below 110 cm (Fig. 4).

^{241}Am, a longer-lived ($T_{1/2}$ = 432 y) decay product of ^{241}Pu, produced by atmospheric nuclear bomb testing, follows the same trend as ^{137}Cs, although with much lower activities, reaching its maximum of 2.76 mBq/g at 101.5 cm, only 1 cm below the ^{137}Cs peak (Fig. 4).

5 Discussion

5.1 The origin of ^{210}Pb excess

^{210}Pb is continuously produced by ^{222}Rn decay in the atmosphere, adsorbed onto aerosol and dust particles and ultimately deposited on the soil surface by rain or snow, or by dust settling ("dry deposition"). In lakes or marine waters, additional adsorbed ^{210}Pb is provided to settling solid particles by decay of ^{222}Rn dissolved in the water column. Except in the case of ^{210}Pb dating of ice or snow accumulation, where ^{210}Pb adsorbed onto detrital particles is negligible, calculation of adsorbed, "excess ^{210}Pb", $(^{210}Pb)_{ex}$, requires a correction based on the so-called

194 "supported ^{210}Pb", i.e. ^{210}Pb assumed to be in radioactive equilibrium with ^{226}Ra inside the
195 detrital component [$(^{210}Pb)_{ex} = (^{210}Pb)_{measured} - (^{226}Ra)_{measured}$].

196 In guano, however, most of the material is made of organics with few detrital particles, as
197 shown by the very low Th contents of the analysed samples (0.4 ppm on average), except in
198 the deepest layers where Th increases up to 3.2 ppm at 138 cm depth. Thus, ^{226}Ra might not
199 originate from a detrital component in secular radioactive equilibrium, but rather be
200 incorporated during the plant-insect-bat cycle, with an unknown (^{210}Pb/^{226}Ra) ratio. On
201 average, (^{226}Ra) amounts to 10% of the measured (^{210}Pb) in the layers mostly devoid of
202 significant detrital minerals (z<108 cm). Thus, the uncertainty linked to the "supported ^{210}Pb"
203 correction should not significantly alter the interpretation of the ^{210}Pb data. It might however
204 contribute partly to the dispersion of the data, as observed in Figure 3.

205 Of more concern is the fact that ^{210}Pb adsorbed on guano might not only come from
206 atmospheric ^{210}Pb fallout, a fraction of which is incorporated during the plant-insect-bat cycle,
207 but also from ^{210}Pb produced by ^{222}Rn decay in the air inside the cave. This can be
208 particularly important in caves where bats only stay for a few months in the year, as in the
209 Brantites III cave. For most of the year, the guano is preserved from direct atmospheric input
210 but can adsorb ^{210}Pb produced by ^{222}Rn decay in the cave air.

211 The relative contributions of these two sources of adsorbed ^{210}Pb could potentially be
212 estimated through the comparison between ^{210}Pb and ^{137}Cs (or ^{241}Am) inventories. The only
213 origin of ^{137}Cs in guano is from atmospheric ^{137}Cs fallout. If we assume that ^{137}Cs and
214 atmospheric $(^{210}Pb)_{ex}$ are fractionated in a similar way during the plant-insect-bat-guano cycle,
215 i.e. if both nuclides have similar "transfer efficiencies" as defined by Robbins and Edgington
216 (1978), then the ratio of their atmospheric inventories, as recorded in soils for example,
217 should be the same as that recorded in the guano, if no other source of adsorbed ^{210}Pb was
218 implied.

219 A ^{137}Cs inventory was measured by Monna et al. (2009) in an undisturbed soil (neoluvisol
220 developed in eolian loess deposits) at an experimental station in Versailles near Paris. These
221 authors found a value of 3200 Bq/m^2 in 1992 (corresponding to 1925 Bq/m^2 in 2014). Le
222 Roux et al. (2010) reported ^{137}Cs inventories in undisturbed soils from Montagne Noire (SW
223 of the French Massif Central), and demonstrated their relationship with the mean annual
224 precipitation (MAP): I_{Cs} (Bq/m^2, in 2007) = 3.04*MAP (mm)-110. The MAP at the Gourdon
225 meteorological station is around 900 mm for the period 1971-2010 (www.infoclimat.fr). With

this value, an inventory of 2626 Bq/m^2 is calculated in 2007, corresponding to 2234 Bq/m^2 in 2014. An approximate value of around 2000 Bq/m^2 can thus be estimated, in agreement with the maps of ^{137}Cs soil inventories recently published by Meusburger et al. (2020).

Atmospheric ^{210}Pb fluxes are reported by Garcia-Orellana et al. (2006) for coastal areas from West-Mediterranean Sea. They also show a good correlation with MAP. Taking into account the MAP measured at Gourdon (900 mm), a flux F of 150 Bq/m^2/y is calculated, resulting in an inventory of 4839 Bq/m^2 ($I = F/\lambda_{Pb}$). A similar value around 5000 Bq/m^2 was obtained from sediments deposited in the Thau lagoon (along the Gulf of Lions coast in France) by Monna et al. (1996). A value slightly above 4000 Bq/m^2 can be derived from a global correlation of ^{210}Pb inventories vs MAP in European inland sites (Appleby 2001; Le Roux, 2008). Taking into account the uncertainties associated with these data, a value of 4500 Bq/m^2 seems a reasonable estimate.

Thus the ratio I_{Pb}/I_{Cs} is 2.25 (4500/2000). The inventories of ^{137}Cs and $^{210}Pb_{ex}$ in the guano deposit can be estimated from our data. They are calculated according to the classical equation:

$$I\ (Bq/m^2) = 10. \sum A(z).\rho(z).\Delta z\ ,$$

where A(z) is the ^{137}Cs or $^{210}Pb_{ex}$ activity/g (in mBq/g) in the layer at depth z (cm), ρ is the "dry bulk density" (g/cm^3) at depth z and Δz (cm) the thickness of layer z. As all the guano layers have not been analysed, activities have been interpolated between measured values, and the average dry bulk density $\bar{\rho}$ used in the estimation, i.e. $I = 10.\ \bar{\rho}.\int_0^\infty A(z).dz$.

The ^{137}Cs inventory (in 2014) in the guano deposit is around 290 Bq/m^2. If the $^{210}Pb_{ex}$ was only derived from atmospheric deposition, as ^{137}Cs, with the same transfer efficiency, one should expect a $^{210}Pb_{ex}$ inventory of 725 Bq/m^2. The value estimated from the curve $(^{210}Pb)_{ex}$ vs depth is around 11700 Bq/m^2, higher by a factor of 16 than the expected value. This strongly suggests that most of the ^{210}Pb adsorbed onto the guano comes from ^{222}Rn decay in the cave air.

^{222}Rn activities/m^3 in cave air are generally much higher than in the atmosphere, due to its release from sediments, residual clays or alterites filling many caves, and to degassing of flowing or dripping waters that were enriched in ^{222}Rn during infiltration through the soil or even through the limestone micro-fractures. While the atmosphere has ^{222}Rn activities of a

few tens of Bq/m^3 (e.g. Gamarini, 2006), ^{222}Rn activities in caves can be a factor of 1000 higher (e.g. Hakl et al., 1997; Cigna, 2005). For example, Guibert et al. (2015) measured a value of 7000 Bq/m^3 for ^{222}Rn in the air of the prehistoric Chauvet cave in France. These authors discuss in detail the mechanisms leading to ^{222}Rn accumulation in the cave. They convincingly demonstrate that ^{210}Pb is enriched at the surface of rock fragments exposed to the cave air, probably from direct adsorption of short-lived nuclides produced by ^{222}Rn decay.

Radon monitoring in a number of caves has revealed large temporal variations at different timescales: diurnal, seasonal, annual and even longer-term variations (e.g. Hakl et al., 1997). It is well known for example that ^{222}Rn activities are higher in the summer than in the winter (Cigna, 2005). During winter, the outside air is generally colder and thus denser than the cave air, and it can invade the cave, whereas during summer the warmer and lighter outside air does not penetrate the cave, allowing ^{222}Rn accumulation. The degree of ventilation of the cave plays an essential role in its ^{222}Rn content and the ^{210}Pb flux produced by ^{222}Rn decay. Ventilation will depend on external factors (temperature, wind…) as well as internal factors linked to the morphology of the cave (e.g. natural or artificial opening or obstruction of conduits modifying air flows). It is thus possible that the usual models of ^{210}Pb dating invoking a constant ^{210}Pb flux (or rate of supply, like in the CF:CS or CRS models) do not apply for the entire period of cave guano deposition.

5.2 Interpretation of $(^{210}Pb)_{ex}$ vs depth profile

As mentioned in section 4.2, we have divided the $(^{210}Pb)_{ex}$ profile into 4 segments, according to Fig. 3. The $^{210}Pb_{ex}$ data of segment 1 (between the surface and 42.5 cm) can not be explained by any classical ^{210}Pb model. Indeed, the "constant rate of supply" (CRS = □) model (Appleby and Oldfield, 1978) is sometimes advocated to explain reverse $^{210}Pb_{ex}$ profiles as a consequence of an acceleration of the accumulation rate w, and thus a decrease in $^{210}Pb_{0,ex}$ initial activity/g A_0 (since A_0= □/□). However, such an abrupt increase in accumulation rate is not supported by the ^{14}C data, which rather suggest a relatively stable rate in the upper part of the guano deposit (after 1963). A possible cause of this peculiar profile would be a sudden decrease in the $^{210}Pb_{ex}$ flux, linked to a decrease in ^{222}Rn concentration in the cave as a consequence of an increased ventilation of the cave with outside air. But such a change occurring during the last 20 years would probably have been noticed by speleologists, who regularly visit the cave to survey the bat population. Another possible explanation is that the adsorbed $^{210}Pb_{ex}$ has been leached from the upper part of the

guano heap. Indeed the upper layers of guano deposits are often characterised by low pH, often below 4 that might result from infiltration of bat's urine and/or microbial decomposition of guano (e.g. Audra et al., 2019; MacFarlane and Lundberg, 2021). In such conditions, $^{210}Pb_{ex}$ might well be leached from the shallow layers and be either accumulated deeper downwards or exported beyond the guano heap. In their recent paper, MacFarlane and Lundberg (2021) argue, on the basis of both natural examples and experimental data, that such a process is probably not uncommon and can affect both ^{210}Pb and ^{137}Cs. In agreement with their conclusion, we suggest that the adsorbed $^{210}Pb_{ex}$ was mobile in the acidic shallower part of the Brantites III guano deposit.

$^{210}Pb_{ex}$ data from segment 2 are compatible with an exponential decrease, despite a large scatter around the best-fit line. They probably reflect a period of approximately constant sedimentation rate, and constant $^{210}Pb_{ex}$ flux (like in the CF:CS model), implying a roughly constant initial $(^{210}Pb)_{0,ex}$ activity/g. The slope ($-\lambda/v$) of the straight line in Fig. 3 indicates a sedimentation rate v of 2.59 ± 0.28 cm/y. This value is very close to the average sedimentation rate obtained from ^{14}C dates for the period 1963-2010 (2.4 cm/y). With such a high sedimentation rate, the analysis of 1cm-thick layers will inevitably lead to a dispersion of the data. Indeed, at an intra-annual scale, the sedimentation rate is not constant, since bats live in the cave and produce guano for only a few months. For the rest of the year, the sedimentation rate is near zero, and the $^{210}Pb_{ex}$ concentration thus much higher at the surface of the fresh guano. In addition, the probable seasonal variation in Radon concentration in the cave will also induce variation in $^{210}Pb_{ex}$ fluxes and concentrations.

A similar CF:CS model can explain the data from segment 4 in Fig. 3. The steeper slope indicates however a much lower sedimentation rate of 0.30 ± 0.04 cm/y. This value is close to that deduced from the two oldest ^{14}C ages (0.39 cm/y). It should be noted that the $^{210}Pb_{ex}$ data of segment 4 are not in continuity with those of segment 2. It means that the initial $^{210}Pb_{0,ex}$ concentration for this older period was different, and higher, compared to that of the younger period. The transition between these two contrasting periods corresponds to segment 3 in Fig. 3, where $(^{210}Pb)_{ex}$ increases with depth.

In summary, $^{210}Pb_{ex}$ data display two distinct stages of guano accumulation, an older one with a low accumulation rate (0.3 cm/y) and a younger one with a much higher rate (2.6 cm/y). Without ^{14}C ages, it would not be possible to assess either the age of this abrupt change, or the deposition date of a particular guano layer. Indeed the only available "anchor point" date,

2011 at the top of the deposit, cannot be used because the mobility of $^{210}Pb_{ex}$ prevents calculation of accumulation rate in the segment 1 zone. However, ^{137}Cs (and ^{241}Am) data provide additional and essential information, as discussed below.

5.3 The essential contribution of ^{137}Cs (and ^{241}Am) profiles

The ^{137}Cs and ^{241}Am profiles displayed in Fig. 4 clearly show the typical profiles expected from the curve of atmospheric fallout of these bomb-related radionuclides (e.g. Barker and Bouisset, 2001). The peak values corresponding to the year 1963 occur between 100 and 102 cm depth for both nuclides and coincides with the ^{14}C date of 1963.4 obtained at 102 cm. Thus ^{137}Cs and ^{241}Am data provide a robust anchor date. Another possible anchor date, although less precisely defined, corresponds to the beginning of significant increase in ^{137}Cs in the atmosphere after the first nuclear tests, i.e. the first years of the 1950-1960 decade. Using these anchor dates and the two accumulation rates determined for stages 2 and 4, an age model can be proposed from the combined ^{210}Pb and ^{137}Cs (^{241}Am) data. The dates calculated from each of the analysed layers are reported in Table 2.

From the $(^{210}Pb)_{ex}$ data and the age of each guano layer obtained from the interpolated ^{14}C ages and the ^{210}Pb-derived accumulation rate for the stage 4, the initial $(^{210}Pb)_{0,ex}$ activities/g, at the time of deposition can be calculated. They are reported in Fig. 5. As expected from Fig. 3, $(^{210}Pb)_{0,ex}$ was higher in the pre-1960 period (around 312 mBq/g) than in the post-1960 period (216 mBq/g). The difference however is small, compared to the large difference in the accumulation rates (an increase by a factor of 8.6). This means that the flux of $^{210}Pb_{ex}$ should have been much lower by a factor of 6 in the pre-1960 period. No major change in climatic conditions is detectable around 1960 in the South of France (Lelièvre et al., 2011). Such a large variation of the flux of $^{210}Pb_{ex}$ in the cave could be explained if there was an abrupt change in the cave ventilation around 1960, i.e. if the cave was largely open to the atmosphere with efficient air circulation and a low Radon concentration before 1960, and was much less ventilated with more Radon accumulation after 1960. Such a change could result for example from the partial closure of the gallery in the distal part of the cave (Fig. 1), as a consequence of rock-fall or sediment discharge obstructing the gallery. Since no direct observation by speleologists is available for this period, it is difficult to go further in this discussion. It should be noted however that such an hypothetical change in cave ventilation might well explain the low accumulation rate (probably resulting from a less numerous bat population), because bats

prefer more stable cave conditions without strong air flows (Zukal et al., 2017; Lüthi and Blant, 2017).

Our data suggest that $^{210}Pb_{ex}$ flux in caves as recorded by guano deposits may vary considerably over time. This implies that great care should be taken before applying the "constant rate of supply" (CRS) model, as sometimes done in the literature (e.g. Bogdanovicz et al., 2020). In order to show that the CRS model would give inaccurate dates in the present case, we have calculated the age of the 1963 layer at 100-102 cm depth, using the classical formula (Appleby and Oldfield, 1978):

$$t = -\frac{1}{\lambda} . \ln (I_t/I_0) ,$$

where I_t and I_0 are the $^{210}Pb_{ex}$ inventories below the layer z (age t), and the total inventory respectively. The calculated age t is 70.6 y (before 2014), i.e. 1943, 20 years older than the true age.

5.4 Comparison of $^{210}Pb_{ex}$, ^{137}Cs (^{241}Am) and ^{14}C age models

In Fig.6 are shown the curves interpolated from ^{14}C dates and $^{210}Pb_{ex}$ and ^{137}Cs - ^{241}Am dates (Table 1). There is a good agreement between the two age models, with a maximum difference of about 5 y in the 1970-1980 AD range (Fig. 6). This shows that $^{210}Pb_{ex}$ data can provide a useful means of dating guano deposits, but that $^{210}Pb_{ex}$ data should be complemented by at least ^{137}Cs data. We thus agree with the recommendation made by Smith (2001) that "^{210}Pb geochronology must be validated using at least one independent tracer", and with the assertion by McFarlane and Lundberg (2021) that the interpretation of $^{210}Pb_{ex}$ data alone will often prove difficult. And, obviously, in spite of its higher analytical cost, ^{14}C remains the best method to date bat guano deposits.

6 Conclusions

The presence, in the Brantites III cave, in SW France, of a relatively thick guano deposit allowed a detailed comparison of the ^{14}C and ^{210}Pb, ^{137}Cs, ^{241}Am dating methods.

The analysed upper part of the guano accumulation was deposited for the last 150 years as indicated by a ^{14}C date obtained for the layer at 138 cm depth. All the other ^{14}C data display $^{14}C/^{12}C$ ratios higher than the value of modern C, clearly indicating that their ages are younger than the introduction in the atmosphere of anthropogenic ^{14}C derived from nuclear tests

(around 1945). Unambiguous ^{14}C ages in stratigraphic order are obtained by comparison with the post-bomb atmospheric curve.

Whereas the origin of ^{14}C ultimately found in the guano is rather straightforward, we show that the origin of ^{210}Pb excesses is more complex. A comparison of $^{210}Pb_{ex}$ and ^{137}Cs inventories derived from atmospheric fallout, and those measured in the guano deposit suggests that most $^{210}Pb_{ex}$ adsorbed onto guano is produced by ^{222}Rn decay inside the cave. As ^{222}Rn concentration in caves might show both short-term (e.g. seasonal) and long-term (several years or more) fluctuations, it can affect the adsorbed $^{210}Pb_{ex}$ flux, making the assumption of a constant rate of supply (in the CRS model) questionable.

The profile of $^{210}Pb_{ex}$ vs depth reveals two contrasting periods of accumulation reflecting large differences in guano accumulation rates (0.3 cm/y before 1960 and 2.6 cm/y after 1960), which agree with the rates derived from ^{14}C ages. Calculation of initial $(^{210}Pb)_{0,ex}$ activities/g indicates a higher activity/g for the older period, but a much lower $^{210}Pb_{ex}$ flux. We tentatively interpret the large difference in fluxes as the result of a relatively abrupt change in cave ventilation from widely open (to the atmosphere) to more confined conditions. This could also explain the smaller number of bats living in the cave before 1960, as suggested by the lower accumulation rate.

The shallower part (30 cm) of the deposit displays a reversed $^{210}Pb_{ex}$ profile that might result from the partial leaching of ^{210}Pb in acidic conditions, as proposed by McFarlane and Lundgren (2021).

Both ^{137}Cs and ^{241}Am activities/g vs depth display simple profiles with a clearly marked peak value at a depth of 100-102 cm, corresponding to 1963, the year of maximum atmospheric fallout. It also coincides with the ^{14}C date obtained for that layer. Using this age and the age of beginning of ^{137}Cs increase (~1952) as anchor ages, and the $^{210}Pb_{ex}$- derived accumulation rates, a combined ^{210}Pb -^{137}Cs - ^{241}Am age model is proposed, which is in good agreement with the ^{14}C age model.

Although the origin of $^{210}Pb_{ex}$ adsorbed on guano deposits is more complex than usually assumed, ^{210}Pb can still be used as a dating tool, when combined with other tracers like ^{137}Cs or ^{241}Am, as demonstrated in this study. Moreover, as $^{210}Pb_{ex}$ is dependent on Radon concentration in the cave air, it can offer insights into past variations in the cave ventilation.

Acknowledgments

The authors would like to warmly acknowledge T. Goslar of the Poznań Laboratory for Radiometric Dating for providing the ^{14}C dates. We are grateful to MISTRAL-BIODIVMEX CNRS program for partially funding the Poznan radiocarbon analyses.

References

Appleby, P.G., Oldfield, F. (1978). The calculation of Lead-210 dates assuming a constant rate of supply of unsupported ^{210}Pb to the sediment. Catena, 5, 1-8.

Appleby, P.G. (2001). Chronostratigraphic techniques in recent sediments. Tracking environmental change using lake sediments. Basin analysis, coring, and chronological techniques. Developments in Paleoenvironmental Research 1, 171–203.

Audra, P., De Waele, J., Bentaleb, I., Chroňáková, A., Krištůfek V., D'Angeli, I.M., Carbone, C., Madonia, G., Vattano, M., Scopelliti, G., Cailhol, D., Vanara, N., Temovski, M., Bigot, J.Y., Nobécourt, J.C., Galli, E., Rull, F., Sanz-Arranz, A. (2019). Guano-related phosphate-rich minerals in European caves. Int. J. of Speleology, 48 (1), 75-105.

Barker, E., Bouisset, P. (2001). Evolution de la radioactivité en France Métropole et en Outre-Mer dans les aérosols et les retombées depuis la mise en place de l'observatoire atmosphérique de l'IPSN. Rapport DPRE/SERNAT/2001-27, 51p.

Bogdanowicz, W., Worobiec, E., Grooms, C., Kimpe, L.E., Smol, J.P., Stewart, R.S., Suchecka, E., Pomorski, J.J. , Blais, J.M., Clare, E.L., Fenton, M.B. (2020). Pollen assemblage and environmental DNA changes: A 4300 year-old bat guano deposit from Jamaica. Quaternary International, 558, 47-58.

Brock, F., Higham, T., Ditchfield, P., Bronk Ramsey, C. (2010). Current pretreatment methods for AMS radiocarbon dating at the Oxford Radiocarbon Accelerator Unit (ORAU). Radiocarbon, 52 (1), 103-112.

Bronk Ramsey, C. (2009). Bayesian analysis of radiocarbon dates. *Radiocarbon, 51*(1), 337–360.

Cigna, A, A. (2005). Radon in caves. International Journal of Speleology, 34 (1-2), 1-18.

Des Marais, D.J., Mitchell, J.M., Meinschein, W.G., Hayes, J.M. (1980). The carbon isotope biogeochemistry of the individual hydrocarbons in bat guano and the ecology of the insectivorous bats in the region of Carlsbad, New Mexico. Geochimica et Cosmochimica Acta, 44(12), 2075-2086.

Ferenc, L.F., Onac, B.P., Tanţău, I., Wynn, J.G., Tămaş, T., Coroiu, I., Giurgiu, A.M. (2015). A Late Holocene environmental history of a bat guano deposit from Romania: an isotopic, pollen and microcharcoal study. Quaternary Science Reviews, 127, 141-154.

Gallant, L.R., Grooms, C., Kimpea, L.E., Smolb, J.P., Bogdanowicz, W., Stewart, R.S., Clare, E.L., Fenton, M.B., Blaisa, J.M. (2020). A bat guano deposit in Jamaica recorded agricultural changes and metal exposure over the last > 4300 years. Palaeogeography, Palaeoclimatology, Palaeoecology 538, 109470.

Galmarini, S. (2006). One year of ^{222}Rn concentration in the atmospheric surface layer. Atmos. Chem. Phys., 6, 2865-2887.

Garcia-Orellana, J, Sanchez-Cabeza, J. A., Masqué, P., Avila, A., Costa, E., Loÿe-Pilot, M.D., Bruach-Menchén, J.M. (2006). Atmospheric fluxes of ^{210}Pb to the western Mediterranean Sea and the Saharan dust influence. J. Geophys. Res., 111, D15305, doi:10.1029/2005JD006660.

Goslar T., Czernik J., Goslar E. (2004). Low-energy ^{14}C AMS in Poznan Radiocarbon Laboratory, Poland. Nuclear Instruments and Methods in Physics Research B 223-224: 5-11.

Guibert, P., Brodard, A., Quiles, A., Geneste, J.M., Baffier, D., Debard, E., Ferrier, C. (2015). When were the walls of the Chauvet-Pont d'Arc Cave heated? A chronological approach by thermoluminescence. Quaternary Geochronology 29, 36-47.

Hakl, J., Hunyadi, I., Csige, I., Géczy, G., Lénart, L., Varhegyi, A. (1997). Radon transport phenomena studied in Karst caves. International experiences on Radon levels and exposures. Radiations Measurements, 28, 1-6, 675-684.

Hua, Q., Turnbull, J. C., Santos, G. M., Rakowski, A. Z., Ancapichún, S., De Pol-Holz, R., Hammer, S., Lehman, S. J., Levin, I., Miller, J. B., Palmer, J. G., & Turney, C. S. M. (2021). Atmospheric Radiocarbon For The Period 1950–2019. Radiocarbon, pp 1–23. doi:10.1017/rdc.2021.95

Johnston, V.E, McDermott, F., Tămaş, T. (2010). A radiocarbon dated bat guano deposit from

N.W. Romania: Implications for the timing of the Little Ice Age and Medieval Climate Anomaly. Palaeogeography, Palaeoclimatology, Palaeoecology, 291(3-4), 217-227.

Lelièvre, F., Sala, S., Ruget, F., Volaire, F. (2011). Evolution climatique du Sud de la France 1950–2009, Projet CLIMFOUREL PSDR3, Régions LR, MP, RA. Série Les Focus PSDR3. (https://www1.montpellier.inra.fr/PSDR/doc/climfourel/FOCUS-PSDR3-CLIMFOUREL_Clim%20Chgt.pdf)

Le Roux, G., Pourcelot, L., Masson, O., Duffa, C., Vray, F., Renaud, P. (2008). Aerosol deposition and origin in French mountains estimated with soil inventories of ^{210}Pb and artificial radionuclides. Atmospheric Environment, 42 (7), 1517-1524.

Le Roux, G., Duffa, C., Vray, F., Renaud, P. (2010). Deposition of artificial radionuclides from atmospheric Nuclear Weapon Tests estimated by soil inventories in French areas low-impacted by Chernobyl. Journal of Environmental Radioactivity, Elsevier, 101, 211-218.

Lüthi, C., Blant, M. (2017). Spéléologie et chauves-souris. (https://www.isska.ch/pdf/Fr/Rd/Biospeleologie/Brochure_Chiro_V3_f.pdf)

Martel, E.A. (1894). Les abîmes : les eaux souterraines, les cavernes, les sources, la spélæologie : explorations souterraines effectuées de 1888 à 1893 en France, Belgique, Autriche et Grèce*, Paris, Librairie Ch. Delagrave, 578 p.*

McFarlane, D.A., Lundberg, J. (2021). Geochronological implications of ^{210}Pb and ^{137}Cs mobility in cave guano deposits. International Journal of Speleology, 50(3), 239-248. https://doi.org/10.5038/1827-806X.50.3.2391

Meusburger, K., Evrard, O., Alewell, C., Borrelli, P., Cinelli, G., Ketterer, M., Mabit, L., Panagos, P., Van Oost, K., Ballabio, C. (2020). Plutonium aided reconstruction of caesium atmospheric fallout in European topsoils. Nature. https://doi.org/10.1038/s41598-020-68736-2

Monna, F. , Lancelot, J., Bernat, M., Mercadier, H. (1996). Taux de sédimentation dans 1' étang de Thau à partir des données géochronologiques, géochimiques et des repères stratigraphiques. Oceanologica Acta, 20, 4, 627-638.

514
515 Monna, F., Van Oort, F., Hubert, P., Dominik, J., Bolte, J., Loizeau, J.L., Labanowski, J.,
516 Lamri, J., Petit, C., Le Roux, G., Château, C. (2009). Modeling of ^{137}Cs migration in soils
517 using an 80-year soil archive: role of fertilizers and agricultural amendments. Journal of
518 Environmental Radioactivity, 100, 9–16.
519
520 Reimer, P., Austin, W., Bard, E., Bayliss, A., Blackwell, P., Bronk Ramsey, C., Butzin, M.,
521 Cheng, H., Edwards, R., Friedrich, M., Grootes, P., Guilderson, T., Hajdas, I., Heaton, T.,
522 Hogg, A., Hughen, K., Kromer, B., Manning, S., Muscheler, R., Palmer, J., Pearson, C., van
523 der Plicht, J., Reimer, R., Richards, D., Scott, E., Southon, J., Turney, C., Wacker, L.,
524 Adolphi, F., Büntgen, U., Capano, M., Fahrni, S., Fogtmann-Schulz, A., Friedrich, R., Köhler,
525 P., Kudsk, S., Miyake, F., Olsen, J., Reinig, F., Sakamoto, M., Sookdeo, A., & Talamo, S.
526 (2020). The IntCal20 Northern Hemisphere radiocarbon age calibration curve (0–55 cal kBP).
527 *Radiocarbon, 62*. (4), 725-757. doi :10.1017/RDC.2020.41
528
529 Robbins, J.A., Edgington, D.N. (1975). Determination of recent sedimentation rates in
530 Lake Michigan using Pb-210 ad Cs-137. Geochim. Cosmochim. Acta, 39, 285-304.
531
532 Smith, J.N. (2001). Why should we believe ^{210}Pb sediment geochronologies? Journal of
533 Environmental Radioactivity, 55, 121–123.
534
535 Vermeesch, P. (2018). IsoplotR: A free and open toolbox for geochronology. Geosci. Front., 9,
536 1479–1493.
537
538 Wirrmann, D., Sémah, A.M., Mendez Millan, M., Schmidt, S., Boissenin, M., Boucher, H.,
539 Bouloubassi, I., Brescia, F., Cetin, F., Djouarev, I., Klein,V. (2017). Signification
540 environnementale de guano de salanganes et de chiroptères de Nouvelle-Calédonie. Premiers
541 résultats. Quaternaire, 28(3), 401-412.
542
543 Wurster, C.M., Patterson, W.P., McFarlane, D.A., Wassenaar, L.I., Hobson, K.A., Athfield,
544 N.B., Bird, M.I. (2008). Stable carbon and hydrogen isotopes from bat guano in the Grand
545 Canyon, USA, reveal Younger Dryas and 8.2 ka events. Geology, 36(9), 683-686.
546

Wurster, C.M., Bird, M.I., Bull, I.D., Bryant, C., Ascough, P. (2009). A protocol for radiocarbon dating tropical subfossil cave guano. Radiocarbon, 51(3), 977-986.

Zukal, J., Berkova, H., Bandouchova, H., Kovacova, V., Pikula, J. (2017). Bats and caves : Activity and ecology of bats wintering in caves. http://dx.doi.org/10.5772/intechopen.69267

Table and Figure captions :

Table 1 : ^{14}C results. Data are reported in « percent Modern Carbon » (pMC) for the period affected by atmospheric nuclear tests. Ages are calculated from the OxCal program (see text for details).

Table 2 : (^{210}Pb), (^{137}Cs) and (^{241}Am) activities/g in the guano samples, calculated in 2014, with their 2 σ uncertainties. ^{14}C ages are reported together with the ages derived from Pb, Cs and Am data. ^{14}C ages in bold characters correspond to the measurements reported in Table 1; the ages in italic are obtained by linear interpolation between two successive ^{14}C dates. The dates in bold characters in the "Pb, Cs, Am dates" column represent anchor dates for the derivation of the age model.

Fig.1: Map of the Brantites III cave. Inset: location of the cave in the SW France.

Fig.2: a) vertical cross-section of the guano deposit. The guano heap is 1.75 m high.

b) Detail showing the staggered arrangement of the cores from C1 at the top to C3 at the bottom. Open black and yellow circles show examples of corresponding layers in C1-C2 and C2-C3 cores, respectively. [colour pictures].

Fig. 3: $(^{210}Pb)_{ex}$ activities/g vs depth. The whole distribution is divided into 4 segments S1 to S4. Only segments 2 and 4 are interpreted as reflecting a roughly constant accumulation rate (2.59 ± 0.28 cm/y and 0.30 ± 0.04 cm/y, respectively). Uncertainties on slopes and derived accumulation rates are calculated using the IsoplotR program (Vermeesch, 2018). Data for S1 are assumed affected by ^{210}Pb mobility (see text for further discussion).

Fig. 4: (^{137}Cs) and (^{241}Am) activities/g vs depth. For clarity, only the average 2 σ uncertainties have been reported.

Fig. 5: Initial $(^{210}Pb)_{0,ex}$ at the time of guano deposition vs age. Note the higher values before 1960. The data for the post-1990 layers are not reported since they are affected by ^{210}Pb mobility (see text for a detailed discussion).

585 Fig. 6: ^{14}C and ^{210}Pb - ^{137}Cs - ^{241}Am age models for the guano deposit.

586

587

^{14}C lab. n°	Sample layer	Depth (cm)	pMC values or age BP	calibrated age AD
Poz-62924	C1 (5-6)	7	105.85 ± 0.33	2005 ± 2
Poz-62926	C2 (5-6)	34.5	113.03 ± 0.31	1993.5 ± 1.5
Poz-134057	C1 (28-29)	37.5	113.77 ± 0.35	1991.5 ± 1.5
Poz-62927	C3 (10-11)	63.5	125.23 ± 0.33	1981 ± 1
Poz-134058	C2 (47-48)	76.5	130.46 ± 0.32	1978.5 ± 0.5
Poz-62928	C4 (10-11)	97	156.37 ± 0.35	1969 ± 1
Poz-134059	C3 (46-47)	102	166.57 ± 0.44	1963.4 ± 0.5
Poz-62929	C4 (50-51)	138	130 ± 30 BP	1871 ± 72

588

589 Table 1

Samples	Depth z (cm)	$(^{210}Pb)_m$ mBq/g	$(^{226}Ra)_m$ mBq/g	$(^{210}Pb)_{ex,2014}$ mBq/g	$(^{137}Cs)_{2014}$ mBq/g	$(^{241}Am)_{2014}$ mBq/g	^{14}C dates (cal AD)	Pb,Cs,Am dates AD	$(^{210}Pb)_{0,ex}$ mBq/g
Top layer	0.0	51.8	4.3	58.9 ± 6.6	<DL	<DL	*2011*	2011	
C1 (0-1)	0.5	41.7	3.2	47.3 ± 5.7	<DL	<DL	*2010*		
C1 (5-6)	7.0	53.5	2.8	62.2 ± 6.5	0.9 ± 0.5	<DL	**2005.0 ± 1.5**		
C1 (11-12)	15.0	64.3	1.5	77.1 ± 6.1	0.2 ± 0.4	<DL	*2001.7*		
C1 (21-22)	28.0	75.8	0.8	92.0 ± 7.8	1.0 ± 0.5	<DL	*1996.2*		
C2 (5-6)	34.5	nd	nd	nd	<DL	<DL	**1993.5 ± 1.5**		
C1 (28-29)	37.5	78.5	1.5	94.6 ± 6.6	<DL	<DL	**1991.5 ± 1.5**		
C2 (13-14)	42.5	95.8	2.8	114.5 ± 7.4	<DL	<DL	*1989.4*	1985.9 ± 5.0	14.71 ± 0.95
C2 (14-15)	43.5	85.8	4.3	101.0 ± 8.7	0.8 ± 0.6	<DL	*1989.0*	1985 ± 4.9	13.13 ± 0.93
C2 (15-16)	44.5	67.2	3.3	78.6 ± 7.4	<DL	<DL	*1988.6*	1985.1 ± 4.8	10.36 ± 0.76
C2 (16-17)	45.5	69.0	2.5	81.9 ± 7.4	<DL	<DL	*1988.2*	1984.7 ± 4.7	10.93 ± 0.79
C3 (10-11)	63.5	62.8	4.8	71.4 ± 5.7	1.2 ± 0.4	<DL	**1981.0 ± 1.0**	1977.7 ± 3.3	11.91 ± 0.61
C2 (47-78)	76.5	63.7	5.8	71.1 ± 5.3	1.1 ± 0.4	<DL	**1978.5 ± 0.5**	1972.7 ± 2.3	12.83 ± 0 .52
C3 (30-31)	85.0	57.2	3.0	67.1 ± 5.4	2.3 ± 0.5	<DL	*1974.7*	1969.5 ± 1.7	13.64 ± 0.73
C3 (39-40)	94.5	51.3	5.3	55.1 ± 5.8	3.3 ± 0.6	<DL	*1970.2*	1965.9 ± 1.1	12.84 ± 0.81
C3 (40-41)	95.5	54.2	10.0	57.4 ± 6.2	3.6 ± 0.6	0.56 ± 0.30	*1969.7*	1965.4 ± 1.1	13.57 ± 0.88
C3 (41-42)	96.5	57.5	11.5	56.3 ± 6.2	4.1 ± 0.7	<DL	*1969.3*	1965.0 ± 1.1	13.52 ± 0.89
C4 (10-11)	97.0	52.3	7.2	58.2 ± 5.1	4.2 ± 0.6	<DL	**1969.0 ± 1.0**	1964.8 ± 1.0	14.09 ± 0.76
C3 (42-43)	97.5	52.8	5.0	59.3 ± 5.8	6.9 ± 0.7	0.86 ± 0.50	*1968.3*	1964.6 ± 1.0	14.71 ± 0.88
C3 (43-44)	98.5	39.5	3.2	45.2 ± 5.0	7.5 ± 0.6	1.44 ± 0.40	*1967.1*	1964.2 ± 1.0	11.78 ± 0.77
C3 (44-45)	99.5	47.5	2.7	55.5 ± 5.8	10.4 ± 0.7	1.66 ± 0.42	*1965.9*	1963.8 ± 1.0	15.20 ± 0.95
C3 (45-46)	100.5	42.3	3.2	48.4 ± 5.8	17.2 ± 1.0	2.07 ± 0.44	*1964.6*	**1963.4 ± 0.5**	14.25 ± 0.88
C3 (46-47)	101.5	39.5	7.2	39.8 ± 5.3	16.5 ± 0.9	2.73 ± 0.50	**1963.4 ± 0.2**	1963.0 ± 1.0	12.01 ± 1.31
C3 (47-48)	102.5	41.7	9.2	40.0 ± 4.1	15.5 ± 0.7	2.18 ± 0.32	*1960*	1962.6 ± 1.0	12.33 ± 1.23
C4 (16-17)	103.0	45.5	16.5	44.3 ± 5.1	12.8 ± 0.8	1.66 ± 0.38	*1959*	1962.5 ± 1.0	13.72 ± 1.42
C3 (48-50)	103.5	40.2	5.2	36.0 ± 5.4	9.0 ± 0.7	1.54 ± 0.42	*1958*	1962.3 ± 1.0	11.29 ± 1.28
C4 (17-18)	104.0	37.3	5.8	39.7 ± 4.2	6.4 ± 0.6	1.25 ± 0.30	*1956*	1961.0 ± 5.0	12.57 ± 1.27
C4 (18-19)	105.0	39.8	4.5	44.8 ± 4.6	3.5 ± 0.6	0.86 ± 0.32	*1954*	1960.0 ± 4.0	14.50 ± 1.46
C4 (19-20)	106.0	42.3	2.3	49.7 ± 5.0	2.5 ± 0.5	0.94 ± 0 .38	*1951*	1959.0 ± 3.0	16.46 ± 1.64
C4 (20-21)	107.0	49.8	4.3	56.5 ± 6.2	3.0 ± 0.7	0.94 ± 0.38	*1949*	1958.2 ± 2.7	19.13 ± 1.92
C4 (21-22)	108.0	43.3	2.8	50.4 ± 4.6	1.7 ± 0.4	0.91 ± 0.36	*1946*	1954.8 ± 2.2	18.93 ± 1.55
C4 (22-23)	109.0	36.0	3.0	41.0 ± 5.4	1.1 ± 0.5	0.19 ± 0.20	*1943*	**1951.5 ± 2.0**	17.10 ± 1.55
C4 (23-24)	110.0	40.3	3.0	46.5 ± 5.0	0.6 ± 0.3	0.31 ± 0.30	*1941*	1948.2 ± 2.2	21.47 ± 1.87
C4 (24-25)	111.0	33.7	6.7	33.5 ± 3.7	0.6 ± 0.4	0.22 ± 0.18	*1938*	1944.8 ± 2.7	17.17 ± 1.73
C4 (39-40)	126.0	20.5	14.3	7.7 ± 4.1	<DL	<DL	*1899*	1895 ± 15	18 ± 10
C4 (50-51)	137.0	30.7	27.0	4.5 ± 7.0	<DL	<DL	**1871 ± 72**	1858 ± 25	34 ± 38

Table 2

Figure 1

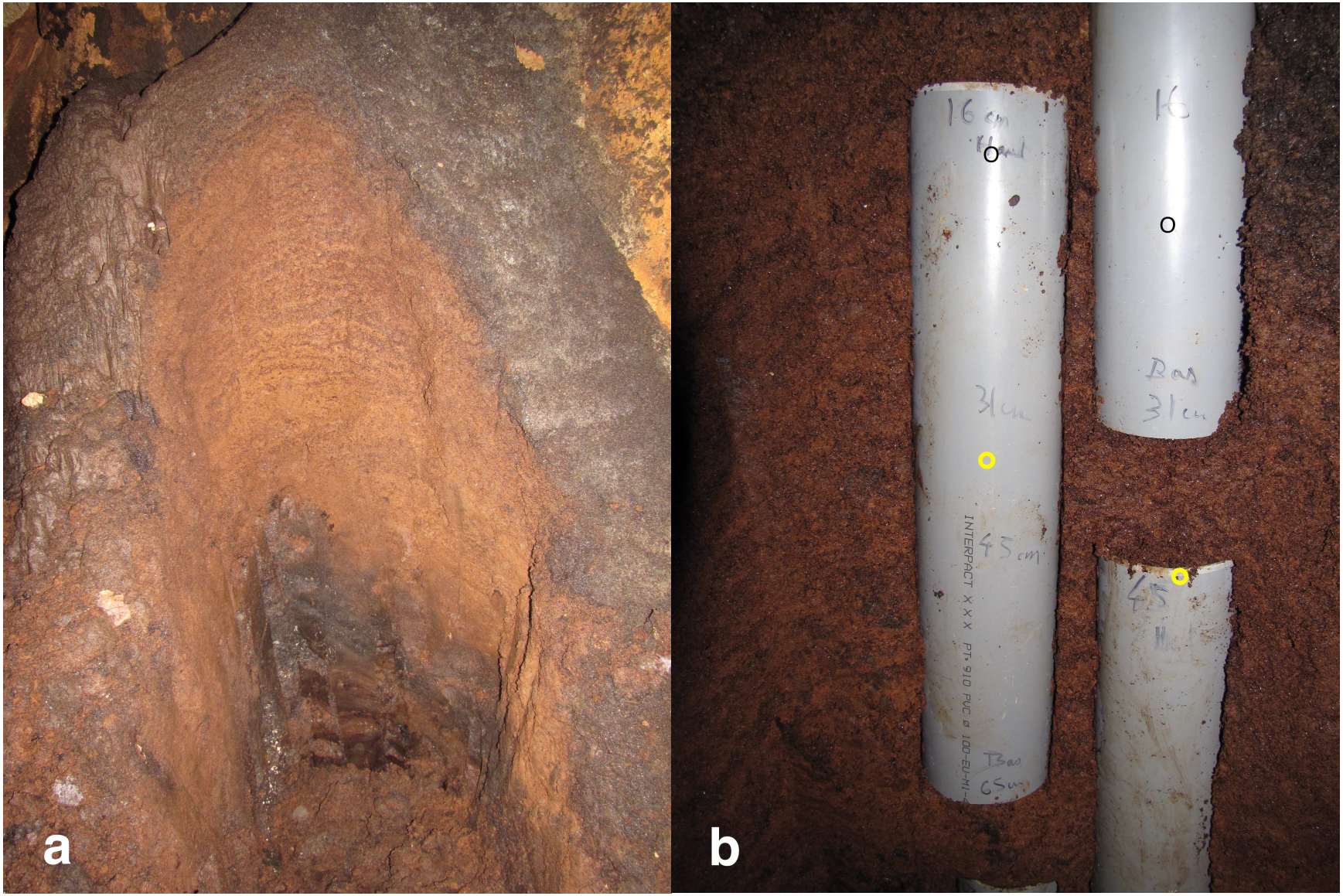

Figure 2

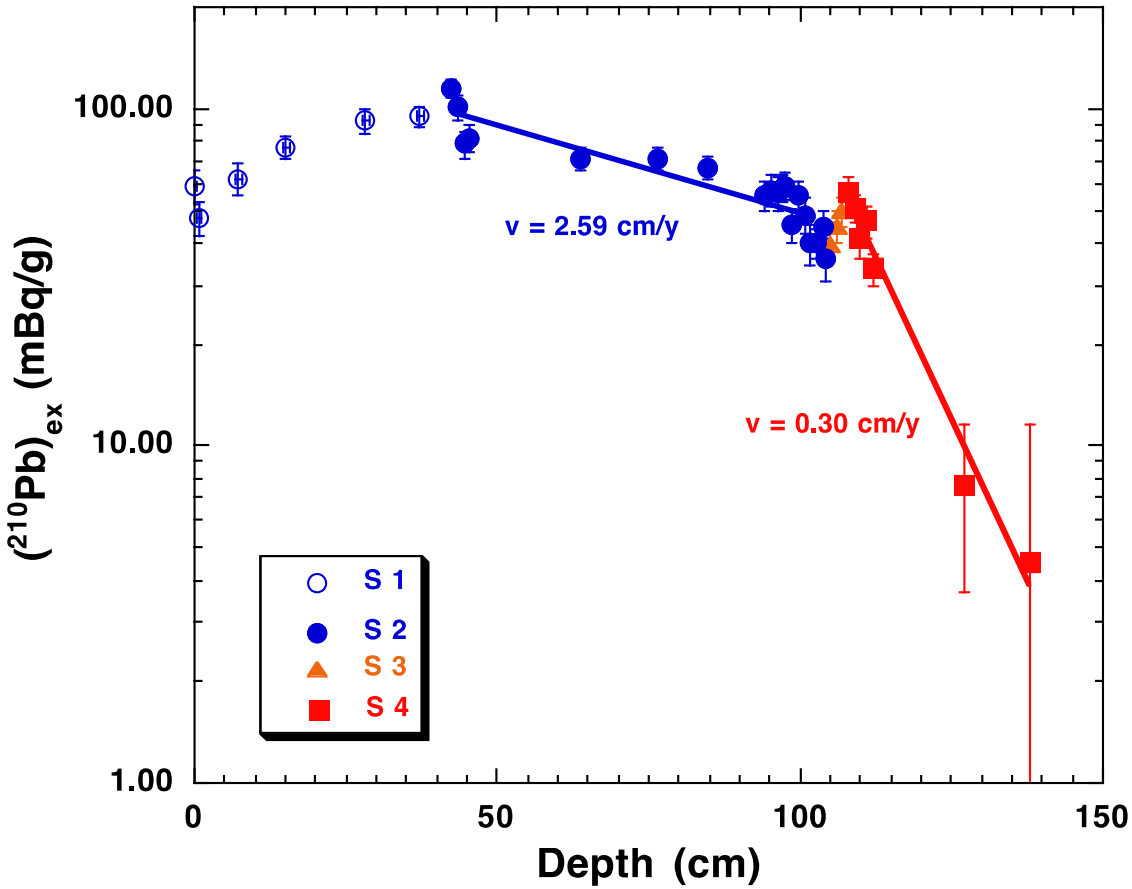
100.00
10.00
1.00
0
50
100
150
Depth (cm)
$(^{210}Pb)_{ex}$ (mBq/g)
v = 2.59 cm/y
v = 0.30 cm/y
S 1
S 2
S 3
S 4

Figure 3

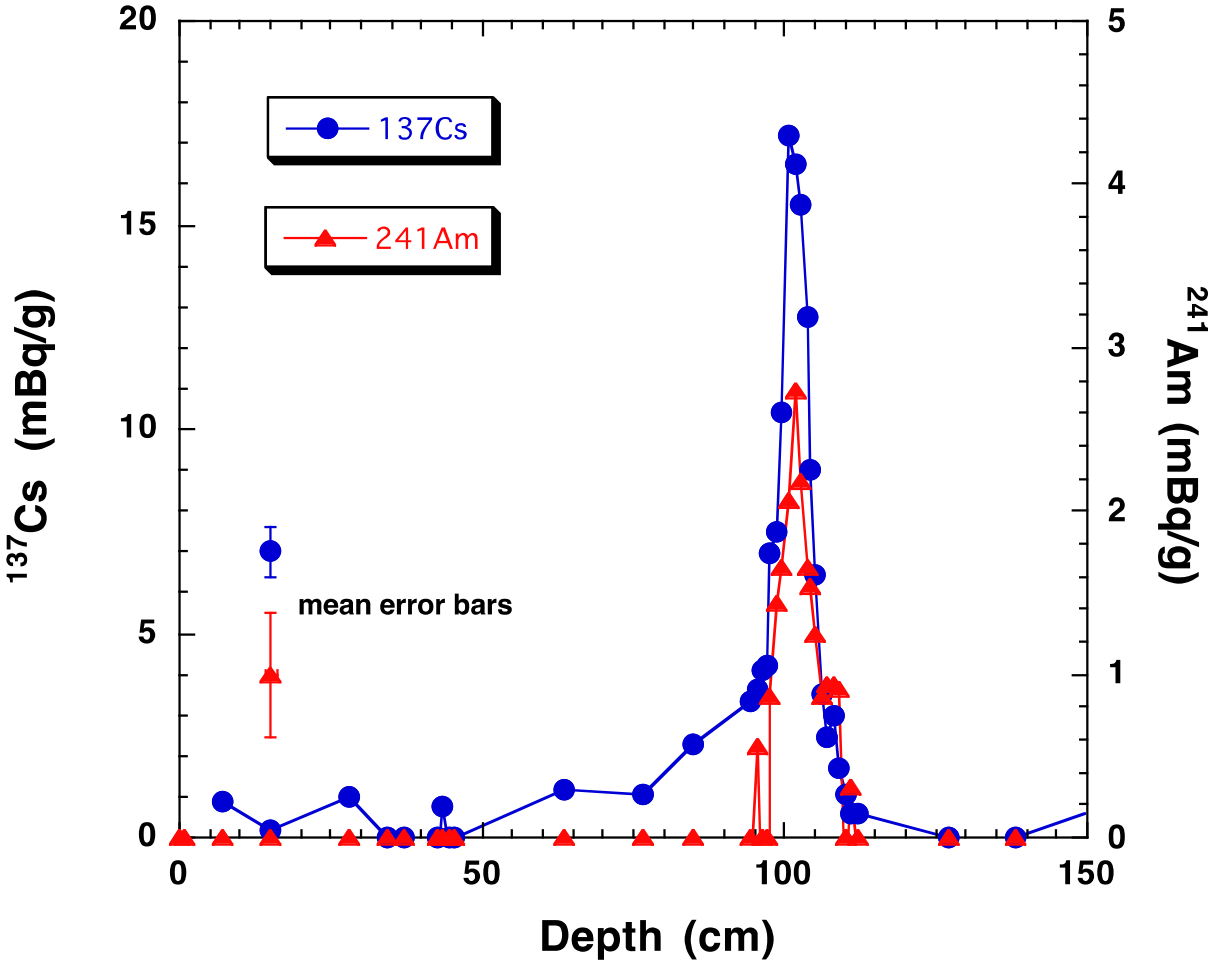
137Cs
241Am
mean error bars
^{137}Cs (mBq/g)
^{241}Am (mBq/g)
Depth (cm)
0
5
10
15
20
0
1
2
3
4
5
0
50
100
150

Fig. 4

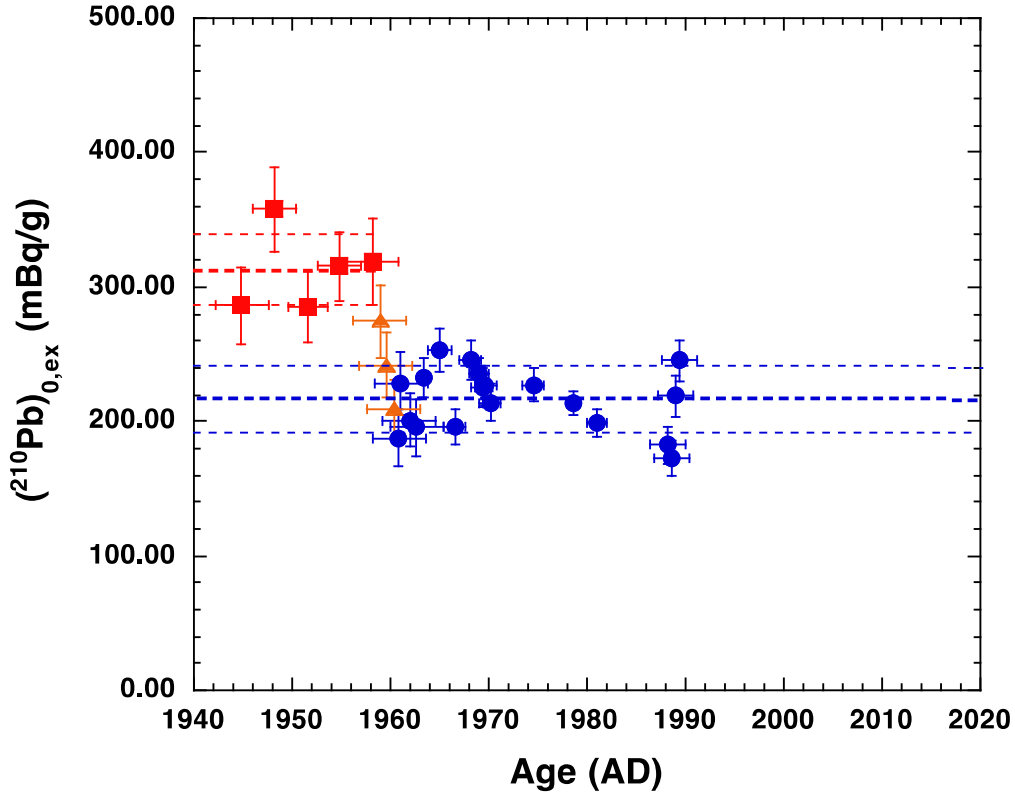
500.00
400.00
300.00
200.00
100.00
0.00
1940
1950
1960
1970
1980
1990
2000
2010
2020
Age (AD)
(210Pb)0,ex (mBq/g)

Fig. 5

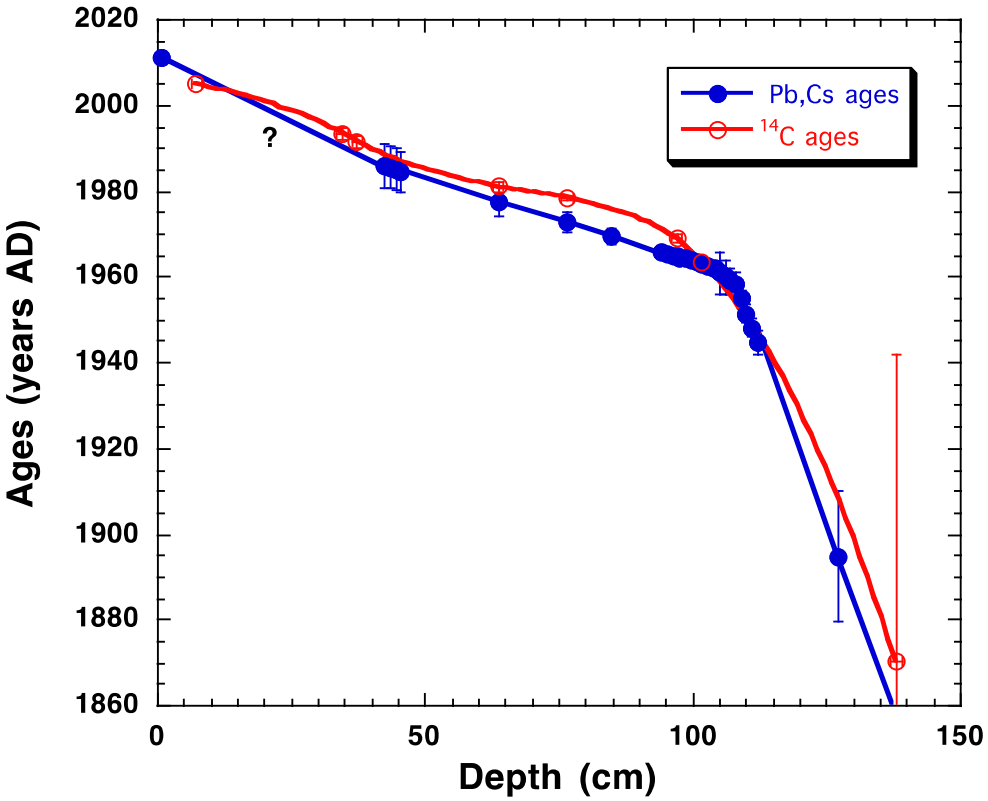
2020
2000
1980
1960
1940
1920
1900
1880
1860
Ages (years AD)
0
50
100
150
Depth (cm)
?
Pb,Cs ages
14C ages

Figure 6